

Nanoscale

Accepted Manuscript



This is an *Accepted Manuscript*, which has been through the Royal Society of Chemistry peer review process and has been accepted for publication.

Accepted Manuscripts are published online shortly after acceptance, before technical editing, formatting and proof reading. Using this free service, authors can make their results available to the community, in citable form, before we publish the edited article. We will replace this *Accepted Manuscript* with the edited and formatted *Advance Article* as soon as it is available.

You can find more information about *Accepted Manuscripts* in the [Information for Authors](#).

Please note that technical editing may introduce minor changes to the text and/or graphics, which may alter content. The journal's standard [Terms & Conditions](#) and the [Ethical guidelines](#) still apply. In no event shall the Royal Society of Chemistry be held responsible for any errors or omissions in this *Accepted Manuscript* or any consequences arising from the use of any information it contains.

Cite this: DOI: 10.1039/c0xx00000x

www.rsc.org/xxxxxx

ARTICLE TYPE

p-Type Dopant Incorporation and Surface Charge Properties of Catalyst-free GaN Nanowires Revealed by Micro-Raman Scattering and X-ray Photoelectron Spectroscopy

Q Wang^a, X Liu^a, M G Kibria^a, S Zhao^a, H P T Nguyen^a, K H Li^a, Z Mi^{*a}, T Gonzalez^b, and M P Andrews^b*Received (in XXX, XXX) Xth XXXXXXXXX 20XX, Accepted Xth XXXXXXXXX 20XX*

DOI: 10.1039/b000000x

Micro-Raman scattering and X-ray photoelectron spectroscopy were employed to investigate Mg-doped GaN nanowires. With the increase of Mg doping level, pronounced Mg-induced local vibrational modes were observed. The evolution of longitudinal optical phonon–plasmon coupled mode, together with detailed X-ray photoelectron spectroscopy studies show that the near-surface region of nanowires can be transformed from weakly n-type to p-type with the increase of Mg doping.

In recent years, one-dimensional semiconductor nanostructures, acting as fundamental building blocks of future devices, have attracted great attentions in the field of nanomaterial and nanotechnology.^{1,2} For example, III-nitride nanowires have been intensively investigated for applications in light emitting diodes, lasers, transistors, biochemical sensors, and solar fuels.^{3–8} Critical for these emerging applications is a precise control of dopant incorporation in such nanostructures. In particular, well controlled p-type doping in III-nitride nanowires is extremely important for achieving highly efficient nanoscale optoelectronic devices.^{9–11} However, compared with doping into bulk materials, doping into semiconductor nanowires is much more complicated due to the large surface-to-bulk volume ratio, the presence of surface states/defects and the possible existence of intrinsic “self-purification” processes.^{12–14} In addition, the doping/free carrier concentration may not be uniform in nanowire structures due to the surface energy band bending, Fermi level pinning, and enhanced surface incorporation/desorption of dopant atoms.^{15–19} For instance, tremendous efforts have been made to understand the impurity doping mechanisms in nanowires grown with the vapor–liquid–solid (VLS) method. It has been revealed that a highly doped shell region tends to be formed in such nanowires, i.e. “surface doping” effect in nanowire structures. This is mainly due to the parasitic growth in the radial direction induced by differences in the precursor decomposition rates between the solid nanowire surface and the catalyst.^{14, 19–21} However, such precursor decomposition is significantly less important in III-V nanowires grown by molecular beam epitaxial (MBE), which may lead to remarkably different surface kinetics and impurity doping processes.^{22–26}

Besides the complexity in doping process itself, characterizing

the doping concentration and doping profile in nanowires is more difficult compared to bulk materials. The traditional magneto-transport methods such as Hall measurements are often not applicable due to the particular contact geometry required by Hall measurements, and, consequently, a detailed understanding of the charge carrier properties of nanowires may not be readily obtained by studying the electrical properties of a single nanowire.^{10, 17, 18, 27–29} In addition, another indirect approach, secondary ion mass spectroscopy (SIMS), typically employed for bulk materials, is not accurate in characterizing nanowires due to its relatively low lateral spatial resolution; and necessary but more complicated planarization process is required to improve the spatial resolution.³⁰ Other characterization methods such as atom probe tomography, Kelvin probe, and capacitance voltage measurements were also employed to investigate the dopant distribution and profile in nanowires. The practicality of these techniques, however, has been severely limited by the very complex process and/or sophisticated facilities required.^{16, 20, 21}

In this regard, simple and contactless micro-Raman scattering spectroscopy is a potential method to study the charge carrier properties and doping distribution of nanowire structures.^{19, 31–33} Recently, there have been a few micro-Raman spectroscopy studies on intrinsic GaN nanowires.^{34–37} Jeganathan et al. investigated the free electron concentration and mobility by analysing the line shape of longitudinal optical phonon–plasmon coupled (LOPC) mode.³⁴ Mata et al. and Wang et al. studied the dependence of surface-related phonon modes and A₁(LO)/QLO modes on a variety of factors.^{36, 37} To date, however, there have been few studies on Mg-doped GaN nanowires by micro-Raman scattering spectroscopy.

In this communication, we performed a comprehensive investigation of GaN nanowires with different Mg doping levels by micro-Raman scattering and angle-resolved X-ray photoelectron spectroscopy (XPS) analysis. In this study, pronounced Mg-induced local vibrational modes (LVMS) were observed in highly Mg-doped GaN nanowires for the first time. Moreover, the transition from the LOPC mode to the uncoupled A₁(LO) phonon mode was clearly measured, suggesting the evolution of the near-surface region of GaN nanowires from weakly n-type to p-type with increasing Mg dopant incorporation. Such a unique surface property evolution is also confirmed by

Cite this: DOI: 10.1039/c0xx00000x

www.rsc.org/xxxxxx

ARTICLE TYPE

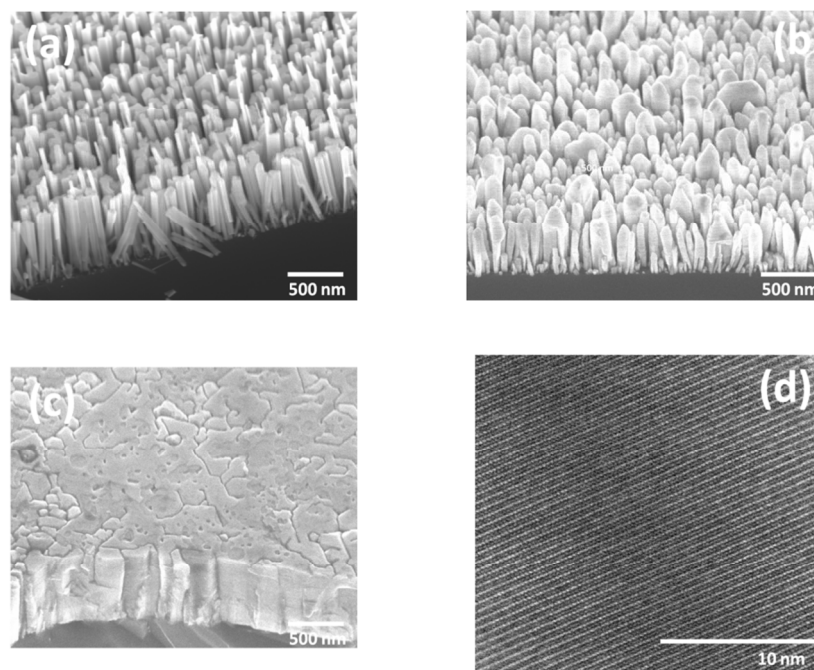


Fig. 1 Typical bird's-eye-view SEM images of GaN nanowires (a) with $T_{Mg}=200\text{ }^{\circ}\text{C}$ (sample A), (b) with $T_{Mg}=265\text{ }^{\circ}\text{C}$ (sample D), and (c) GaN epilayer with $T_{Mg}=230\text{ }^{\circ}\text{C}$ (sample F). (d) High resolution TEM image of sample B

detailed XPS analysis. Consequently, this result can well explain the commonly measured downward surface band bending for p-type GaN.

Catalyst-free GaN nanowires were grown on Si (111) substrates using a Veeco Gen II radio frequency plasma-assisted MBE system under nitrogen rich conditions. Before the growth initiation, a thin Ga seeding layer was firstly deposited in situ, which can promote the formation of GaN nanowires vertically aligned on the Si substrate. The substrate temperature was kept at $\sim 780\text{ }^{\circ}\text{C}$, and the nanowire axial growth rate was $\sim 3\text{ nm/min}$. The Mg doping level in nanowires was controlled by varying the Mg cell temperature (T_{Mg}) from $200\text{ }^{\circ}\text{C}$ to $280\text{ }^{\circ}\text{C}$. Samples A, B, C, D and E correspond to T_{Mg} of $200\text{ }^{\circ}\text{C}$, $230\text{ }^{\circ}\text{C}$, $250\text{ }^{\circ}\text{C}$, $265\text{ }^{\circ}\text{C}$, and $280\text{ }^{\circ}\text{C}$, respectively. The Mg dopant concentration for samples A, B, C, and D are estimated to be $\sim 2.8 \times 10^{18}$, 2.4×10^{19} , 1.0×10^{20} , and $2.9 \times 10^{20}\text{ cm}^{-3}$, respectively, which was derived based on the SIMS performed on Mg-doped GaN epilayers grown under similar conditions and variations of the Mg beam flux at different temperatures. The Mg dopant concentration in nanowire structures may vary from the estimated values, due to surface segregation and/or desorption of dopant atoms. Structural properties of nanowires were examined using a high-resolution scanning electron microscope (SEM) with an acceleration voltage of 5 kV. The representative SEM images of GaN nanowires with $T_{Mg}=200\text{ }^{\circ}\text{C}$ (sample A) and $T_{Mg}=265\text{ }^{\circ}\text{C}$ (sample D) are shown in Figs. 1(a) and 1(b), respectively. It is seen GaN nanowires are vertically aligned on the substrate. With the increase of Mg

doping level, diameters of nanowires become larger and some nanowires are coalesced due to enhanced radial growth with the incorporation of Mg atoms.^{3, 35, 38-40} A Mg-doped GaN epilayer structure (sample F) with the T_{Mg} of $230\text{ }^{\circ}\text{C}$ was also grown and studied. The SEM image of sample F is shown in Fig. 1(c). A typical high resolution transmission electron microscopy (TEM) image of Mg-doped GaN nanowires (sample B) is presented in Fig. 1(d). No extended defects or dislocations can be observed in such single crystalline nanowires. The distance between the two adjacent atomic layers is estimated to be about $\sim 0.52\text{ nm}$ confirming that nanowires are of wurtzite crystal structure, with the c axis (0001) aligned along the growth direction.

Micro-Raman measurements were carried out at room-temperature with an external 488 nm Argon ion laser through a $100\times$ objective with a numerical aperture ~ 0.9 . The focused laser spot size was $\sim 1\text{ }\mu\text{m}$ and the estimated power on the sample was $\sim 40\text{ mW}$. The Raman signal was detected by a Synapse CCD detector mounted on a Horiba LabRam HR confocal Raman spectrometer. In this study, all Raman spectra were taken in the backscattering geometry with the incident laser parallel with the hexagonal c-axis ([0001] direction) of the nanowires. The laser light was scattered without polarization analysis ($z(\cdot)z$ direction) and dispersed with a $1200\text{ g}\cdot\text{mm}^{-1}$ grating. The resolution of a given peak position under these conditions is on the order of 0.02 nm . Typical room-temperature Raman microprobe spectra of GaN nanowires with different Mg doping levels (samples A-E) are presented in Fig. 2(a) (from 300 to 770 cm^{-1}) and Fig. 2(b)

Cite this: DOI: 10.1039/c0xx00000x

www.rsc.org/xxxxxx

ARTICLE TYPE

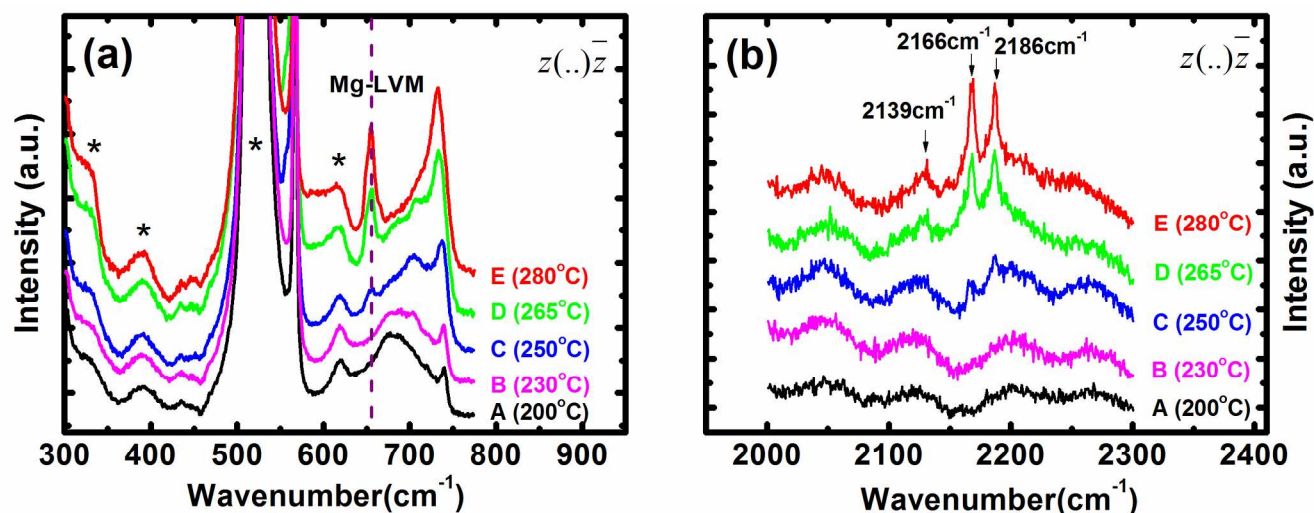


Fig. 2 Typical micro-Raman spectra of GaN nanowires (a) between 300 cm^{-1} to 770 cm^{-1} and (b) between 2000 cm^{-1} to 2300 cm^{-1} with T_{Mg} ranging from 200 $^{\circ}\text{C}$ to 280 $^{\circ}\text{C}$. Si modes are pointed out with * and the dashed lines are guides for the eye. The spectra are vertically shifted for display purpose.

(from 2000 to 2300 cm^{-1}), respectively. For all samples strong Si
 5 signal at 520 cm^{-1} and the GaN E_2 mode are dominant (spectra
 presented here are scaled out to show the weaker modes more
 clearly). Shown in Figs. 2 (a) and (b), distinct spectral evolution
 can be observed for nanowires with different Mg doping levels.

Firstly, with an increase in Mg doping level, a new mode at
 10 655 cm^{-1} begins to appear in sample C ($T_{\text{Mg}}=250$ $^{\circ}\text{C}$), as shown
 in Fig. 2(a). Its intensity becomes stronger with increasing Mg
 doping in samples D ($T_{\text{Mg}}=265$ $^{\circ}\text{C}$) and E ($T_{\text{Mg}}=280$ $^{\circ}\text{C}$). The
 appearance of this Raman mode is related to the LVM associated
 15 with Mg impurity, which replaces the heavier host-lattice (Ga)
 atom and induces a localized atomic oscillation.^{41, 42} The
 frequency of this LVM mode can be estimated by using the
 valence-force model of Keating and Kane and scaling-factor
 approximation. With an appropriate cluster scaling factor (-0.15),
 the frequency for one of the Mg-N vibrations is estimated to be
 20 ~ 660 cm^{-1} ^{42, 43}, which is very close to the presented LVM in Fig.
 2(a). This is the first report on the observation of such Mg-
 induced LVM in GaN nanowire structures and it is in quantitative
 agreement with previous reports on Mg-doped GaN epilayers.<sup>41,
 44, 45</sup> Moreover, shown in the Raman spectra around 2200 cm^{-1} in
 25 Fig. 2(b), three distinct modes at 2139 cm^{-1} , 2166 cm^{-1} and 2186
 cm^{-1} are detected for nanowire samples with T_{Mg} above 250 $^{\circ}\text{C}$.
 These spectroscopic features can be attributed to the LVM
 associated with Mg-H complexes or H-decorated nitrogen
 vacancies.^{42, 44, 46, 47} The presence of these Mg-induced foreign
 30 modes at 655 cm^{-1} and ~ 2200 cm^{-1} are directly linked to the
 acceptor level concentration and could be employed to evaluate
 the incorporation of Mg dopant atoms/hole concentration, as
 shown in previous studies in Mg-doped GaN epilayers.^{41, 42, 47}

Therefore, the absence of LVMs in samples A and B can be
 35 attributed to the low Mg doping level in nanowires, due to
 relatively low Mg cell temperatures and the predominant surface
 desorption of Mg atoms during the epitaxial growth process,
 which will be discussed in detail later.⁹ Such dopant surface
 desorption process could be gradually compensated with further
 40 increased T_{Mg} (250 $^{\circ}\text{C}$ and higher), and thus acceptor
 incorporation can be significantly enhanced. This is confirmed by
 the presence of LVM in samples C, D and E.

Now let us focus on the evolution of the Raman mode at 730-
 740 cm^{-1} with increasing Mg doping level. Shown in Fig. 2(a), for
 45 nanowires with the lowest Mg doping level (sample A with
 $T_{\text{Mg}}=200$ $^{\circ}\text{C}$), a broad band centred at about 680-700 cm^{-1} and a
 mode at 740.2 cm^{-1} are presented. The broad peak here
 corresponds to the SO phonon mode, which is related to
 oscillations of atoms on the free surfaces of polar semiconductors
 and is sensitive to the morphology, size, and density of
 50 nanowires.^{36, 37} More importantly, the mode around 740.2 cm^{-1} is
 attributed to the coupling between the longitudinal optical phonon
 and electron plasmon (LOPC mode), when the plasma frequency
 is in the range of the phonon frequency. Previously, a similar
 55 LOPC mode was also identified in undoped GaN nanowires
 where it was associated with the coupling between the LO
 phonon and the background electron plasmon.^{34, 35} Generally
 speaking, the LOPC mode shifts further to a higher frequency
 with increasing electron concentration and its intensity becomes
 60 weaker. In n-type GaN epilayers, the shift of LOPC mode can
 reach up to a few tens of cm^{-1} wavenumber when the electron
 density increases from 10^{17} to 10^{19} cm^{-3} .⁴¹ In case of Mg doped

Cite this: DOI: 10.1039/c0xx00000x

www.rsc.org/xxxxxx

ARTICLE TYPE

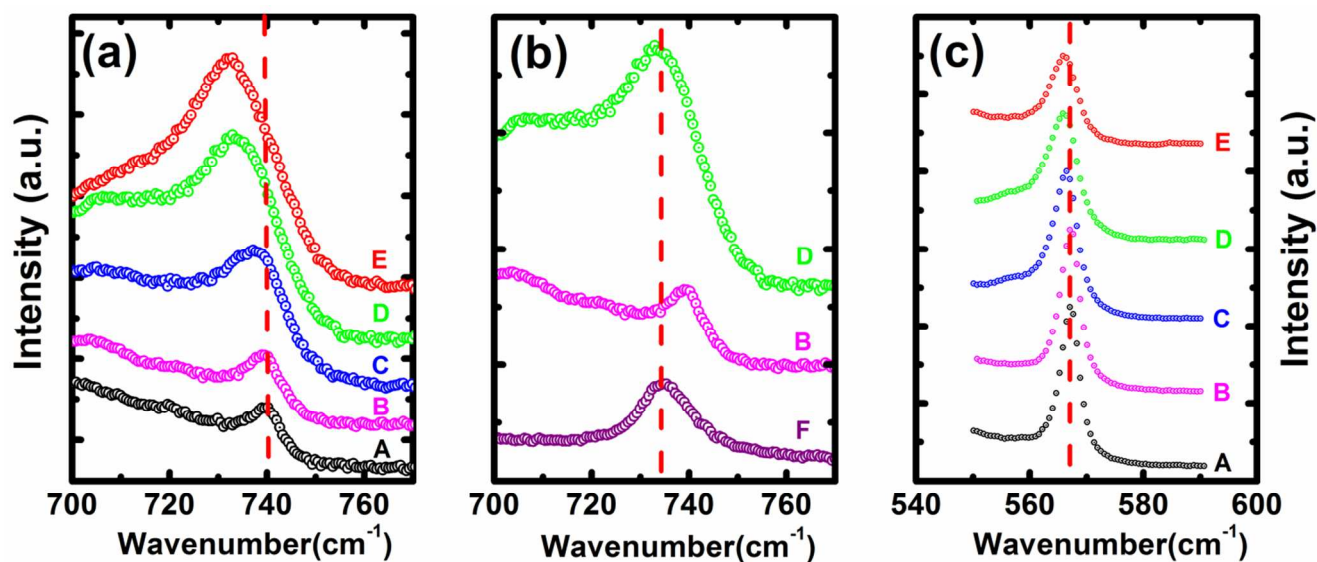


Fig. 3 (a) Micro-Raman spectra in adapted scale focusing on LOPC mode. (b) Micro-Raman spectra of GaN nanowires (sample B) and epilayer (sample F) with the same Mg doping level, and GaN nanowires with a higher doping level (sample D). (c) Micro-Raman spectra in adapted scale focusing on the E_2 mode. (Dashed lines are guides for the eye.)

III-nitride nanowires grown by MBE, the desorption of Mg atoms mainly occurs near the surface region of nanowires, although the formation energy of Mg-doping at the surface of nanowires is significantly lower than that in the bulk region.⁹ This could lead to the formation of surface defects/states and thus make the nanowire surface become weakly n-type. It needs to mention that GaN nanowires are almost transparent to 488 nm excitation laser. In this case, due to the inhomogeneous distribution of charge carriers in the lateral direction of nanowires, i.e. the presence of surface electron, the measured Raman spectra were expected to show both the LOPC mode associated with the bulk and surface region, respectively. In order to simplify the analysis and highlight the key physical evolution of the LO-plasmon coupling process, we will mainly focus on the overall plasmon coupling effect. In sample A, plasmons induced by accumulated surface electrons and bulk background electron can readily interact with LO phonons, forming the presented obvious LOPC mode. With the increase of T_{Mg} , the surface dopant desorption process can be effectively compensated by enhanced acceptor incorporation in the near-surface region due to the lower formation energy. Accordingly, the accumulated surface electrons could be significantly reduced and thus eventually result in the appearance of p-type nanowire surface. Background electrons in the bulk region of nanowires will also be effectively compensated. Such Mg doping mechanism in GaN nanowires is supported by the evolution of the LOPC mode with different Mg doping levels presented in Fig. 3(a). It can be observed that with increasing Mg doping in samples B ($T_{Mg}=230$ °C), C ($T_{Mg}=250$ °C) and D ($T_{Mg}=265$ °C), the frequency of the LOPC mode gradually shifts to lower wavenumbers, i.e. 739.0 cm^{-1} , 737.2 cm^{-1} , and 732.9 cm^{-1} ,

respectively. Such a significant redshift of frequency is mainly due to the reduced coupling between the LO phonon and the weakened surface electron plasmon. Accordingly, the intensity of the LOPC mode also becomes stronger. However, any further shift of the LOPC mode is almost negligible in Sample E compared with that of sample D. This indicates the coupling between the LO phonon and surface (also bulk background) electron plasmon is completely suppressed in these two more heavily Mg doped nanowire samples. Importantly, it indicates that the surfaces of samples D and E are completely transformed from weakly n-type to p-type with the increase of Mg doping, which is also well correlated with the strong Mg-LVM peak at 655 cm^{-1} and around 2200 cm^{-1} in these two samples, shown in Figs. 2(a) and (b). Such a conclusion is unambiguously confirmed by detailed XPS studies, which will be discussed later.

It is also worth noting that in Fig. 2(a) increasing the Mg doping causes a significant change of the SO phonon mode. As also reported previously by Mata et al. and Wang et al, this may be due to the modification of density, morphology and filling factor of nanowires with different Mg doping levels (see Fig. 1).^{36,37} The incorporation of Mg is known to enhance the lateral growth of GaN nanowires, leading to larger diameters and increased coalescence.^{35, 39, 40} However, in Mata et al. and Wang et al's reports, the frequency of A_1 (LO)/QLO mode has no obvious shift indicating that such modifications in GaN nanowire structures have negligible effect on the LO mode.^{36, 37} In turn, it further confirms that the observed significant change of LO in Mg doped GaN nanowires is directly associated with the plasmon coupling effect. However, it also needs to mention that the reduced surface-to-volume ratio will decrease the number of

surface electrons and this may facilitate the suppression of the LOPC mode intensity and yield the uncoupled $A_1(\text{LO})$ mode to some extent.

In order to add further support to the above explanation about the evaluation of the LOPC mode, the Raman spectrum of a GaN epilayer (sample F) with the same Mg doping level as sample B ($T_{\text{Mg}}=230^\circ\text{C}$) was also measured under the same conditions. The result is shown in Fig. 3(b). We observed that only the E_2 mode and the uncoupled $A_1(\text{LO})$ mode were present for the Mg doped GaN epilayer. The absence of the broad SO phonon mode around 700 cm^{-1} is due to the massively reduced surface-to-volume ratio compared with that of the nanowires (sample B). More importantly, the frequency of the uncoupled $A_1(\text{LO})$ mode in this epilayer sample is almost identical to the $A_1(\text{LO})$ mode in sample D ($T_{\text{Mg}}=265^\circ\text{C}$), confirming the absence of interaction between the LO and surface electron plasmon in heavily Mg-doped nanowires.

Moreover, it is likely that the shift of Raman mode can be induced by doping dependent changes in strain in nanowires. Manifestations of this show up by examining the shift in the peak position of the E_2 mode, which is sensitive to the biaxial strain in the c -plane. Shown in Fig. 3(c), the shift of the E_2 mode between sample A and sample E is about $\sim 1\text{ cm}^{-1}$ due to the increased tensile strain at higher Mg doping levels. Such strain-induced shift is expected to be even smaller for the $A_1(\text{LO})$ mode,⁴⁸ which is almost negligible compared with the measured shift of the $A_1(\text{LO})$ shown in Fig. 3(a). Therefore, it confirms that the shift of the $A_1(\text{LO})$ in nanowires with different Mg doping levels is mainly due to the decoupling of the LOPC mode rather than doping induced strain. Moreover, sample A is associated with the highest E_2 mode frequency ($\sim 567.1\text{ cm}^{-1}$), close to that exhibited by freestanding GaN, indicating effective strain relaxation in the lateral direction of nanowires. Accordingly, it shows a higher crystal quality confirmed by a narrower full-width-at-half-maximum (FWHM) of the E_2 peak ($\sim 5\text{ cm}^{-1}$). The broader FWHM of the E_2 peak of sample E (more than 10 cm^{-1}) is probably related to structural degradation caused by increased Mg doping.

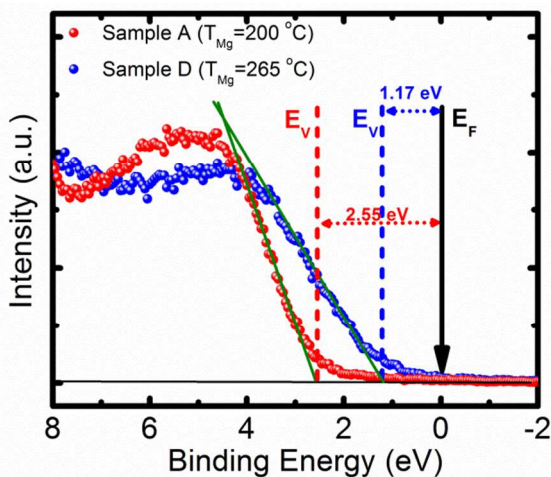


Fig. 4. X-ray photoelectron spectroscopy of Mg-doped GaN nanowires with $T_{\text{Mg}}=200^\circ\text{C}$ (sample A) and $T_{\text{Mg}}=265^\circ\text{C}$ (sample D), from which the values of $E_{\text{F}}-E_{\text{V}}$ can be derived.

The surface energy band structure of Mg-doped GaN

nanowires were characterized by angle-resolved XPS. In order to obtain the majority signal from the sidewall of nanowires, an X-ray beam was impinged with a 60 degree angle with respect to the growth direction of nanowires (0001). During the measurement, Au-4f peak (84 eV) and C-1s peak (285 eV) were used to calibrate the valence band spectra. For the undoped GaN nanowire sample, the energy separation between the near-surface Fermi-level and the valence band maximum ($E_{\text{F}}-E_{\text{V}}$) is measured to be 2.63 eV, similar to that of n-type GaN surfaces by Wu et al and that of non-doped GaN nanowires by Calarco et al.^{18,26,49} Figure 4 presents typical XPS spectra of nanowires with two different doping levels, i.e. sample A ($T_{\text{Mg}}=200^\circ\text{C}$) and sample D ($T_{\text{Mg}}=265^\circ\text{C}$). It can be observed that, for sample A, the $E_{\text{F}}-E_{\text{V}}$ is about 2.55 eV, suggesting that the surface of GaN nanowires grown with relatively low T_{Mg} is weakly n-type. In contrast, for sample D, the near-surface Fermi level shifts noticeably toward the VBM, with the $E_{\text{F}}-E_{\text{V}}$ being reduced to about 1.17 eV. Evidently, the surface of nanowires is transformed from weakly n-type to p-type with increasing Mg cell temperature. The reduction of $E_{\text{F}}-E_{\text{V}}$ in the near surface region can be directly correlated to the reduction in the downward surface band bending with increasing Mg-dopant incorporation. Such band bending is approximately the shift of the Fermi level, since the change of Fermi level in the bulk region is much smaller than that in the surface region at high doping level.²⁶ More detailed analysis of the surface charge properties of GaN:Mg nanowires can be found in previous publications.²⁶

Table I. $E_{\text{F}}-E_{\text{V}}$, LOPC mode frequency and the presence of LVMS vs. T_{Mg} .

| T_{Mg} | 200°C | 230°C | 250°C | 265°C | 280°C |
|---|---------------------|---------------------|---------------------|---------------------|---------------------|
| $E_{\text{F}}-E_{\text{V}}$ (eV) | 2.55 | 2.45 | 1.90 | 1.17 | 0.67 |
| ω_{LOPC} (cm^{-1}) | 740.2 | 739.0 | 737.2 | 732.9 | 732.9 |
| LVMS | absent | absent | weak | strong | strong |

Finally, table I shows the summary on the values of $E_{\text{F}}-E_{\text{V}}$ derived from XPS, the frequency of the LOPC mode, and the presence of Mg induced-LVMS measured by Raman spectra for different T_{Mg} . It can be observed that the values of $E_{\text{F}}-E_{\text{V}}$ are approximately the same at relatively low T_{Mg} (samples A and B), wherein the surface Mg desorption process dominates. It results in a weakly n-type surface of nanowires, which is well correlated with the commonly measured downward surface band bending for p-type GaN.⁵⁰⁻⁵³ This unique phenomena also leads to the coupling between the LO phonon and surface electron plasmon presented in the Raman spectra. Such accumulated surface electrons are gradually compensated by enhanced Mg incorporation with higher T_{Mg} . It leads to the decoupling of the LOPC mode and eventually the presence of p-type nanowire surface, as shown in Table I.

Conclusions

In summary, we have performed a detailed investigation of the structural and surface charge properties of GaN:Mg nanowires and have identified that Mg dopant incorporation in GaN nanowires is highly non-uniform across the nanowire lateral dimension, due to the enhanced surface desorption of dopant atoms. As such, the surface of GaN:Mg nanowires is weakly n-type and characterized by the presence of surface electrons at

relatively low doping levels. Such weakly n-type surface can be transformed to p-type with increasing Mg dopant incorporation. A detailed understanding of this doping process provides a unique opportunity to engineer the surface charge properties of nanowires for their emerging applications in nanophotonics and electronics.

Acknowledgements

This work is supported by the Natural Sciences and Engineering Research Council of Canada and the Fonds de recherche sur la nature et les technologies. The authors wish to thank Dr. Omid Salehzadeh at McGill University for useful discussions.

Notes and references

^a Department of Electrical and Computer Engineering, McGill University, 3480 University Street, Montreal, QC H3A 0E9, Canada Fax: +1-514-398-4470; Tel: +1-514-398-7114.

* E-mail: zetian.mi@mcgill.ca

^b Department of Chemistry, McGill University, 801 Sherbrooke St West, Montreal, QC H3A 0B8, Canada

1. Y. Cui and C. M. Lieber, *Science*, 2001, **291**, 851-853.
2. W. Lu and C. M. Lieber, *Nat. Mater.*, 2007, **6**, 841-850.
3. S. F. Li and A. Waag, *J. Appl. Phys.*, 2012, **111**.
4. P. Yang, R. Yan and M. Fardy, *Nano Lett.*, 2010, **10**, 1529-1536.
5. M. H. Huang, S. Mao, H. Feick, H. Yan, Y. Wu, H. Kind, E. Weber, R. Russo and P. Yang, *Science*, 2001, **292**, 1897-1899.
6. M. G. Kibria, H. P. T. Nguyen, K. Cui, S. Zhao, D. Liu, H. Guo, M. L. Trudeau, S. Paradis, A.-R. Hakima and Z. Mi, *ACS Nano*, 2013, **7**, 7886-7893.
7. H. P. T. Nguyen, S. Zhang, A. T. Connie, M. G. Kibria, Q. Wang, I. Shih and Z. Mi, *Nano Lett.*, 2013, **13**, 5437-5442.
8. K. A. Bertness, N. A. Sanford and A. V. Davydov, *IEEE J. Sel. Topics Quantum Electron.*, 2011, **17**, 847-858.
9. S. Zhao, B. H. Le, D. P. Liu, X. D. Liu, M. G. Kibria, T. Szkopek, H. Guo and Z. Mi, *Nano Lett.*, 2013, **13**, 5509-5513.
10. Z. Zhong, F. Qian, D. Wang and C. M. Lieber, *Nano Lett.*, 2003, **3**, 343-346.
11. S. W. Kim, Y. H. Park, I. Kim, T.-E. Park, B. W. Kwon, W. K. Choi and H.-J. Choi, *Nanoscale*, 2013, **5**, 8550-8554.
12. J. Wallentin and M. T. Borgström, *J. Mater. Res.*, 2011, **26**, 2142-2156.
13. G. M. Dalpian and J. R. Chelikowsky, *Phys. Rev. Lett.*, 2006, **96**, 226802.
14. D. J. Norris, A. L. Efros and S. C. Erwin, *Science*, 2008, **319**, 1776-1779.
15. S. Zhao, S. Fatholouloumi, K. H. Bevan, D. P. Liu, M. G. Kibria, Q. Li, G. T. Wang, H. Guo and Z. Mi, *Nano Lett.*, 2012, **12**, 2877-2882.
16. E. Koren, J. K. Hyun, U. Givan, E. R. Hemesath, L. J. Lauhon and Y. Rosenwaks, *Nano Lett.*, 2010, **11**, 183-187.
17. J.-R. Kim, H. M. So, J. W. Park, J.-J. Kim, J. Kim, C. J. Lee and S. C. Lyu, *Appl. Phys. Lett.*, 2002, **80**, 3548-3550.
18. R. Calarco, M. Marso, T. Richter, A. I. Aykanat, R. Meijers, A. v.d. Hart, T. Stoica and H. Lüth, *Nano Lett.*, 2005, **5**, 981-984.
19. N. Fukata, S. Ishida, S. Yokono, R. Takiguchi, J. Chen, T. Sekiguchi and K. Murakami, *Nano Lett.*, 2011, **11**, 651-656.
20. D. E. Perea, E. R. Hemesath, E. J. Schwabach, J. L. Lensch-Falk, P. W. Voorhees and L. J. Lauhon, *Nat. Nano.*, 2009, **4**, 315-319.
21. E. C. Garnett, Y.-C. Tseng, D. R. Khanal, J. Wu, J. Bokor and P. Yang, *Nat. Nano.*, 2009, **4**, 311-314.
22. J. Dufouleur, C. Colombo, T. Garma, B. Ketterer, E. Uccelli, M. Nicotra and A. Fontcuberta i Morral, *Nano Lett.*, 2010, **10**, 1734-1740.
23. C. Colombo, D. Spirkoska, M. Frimmer, G. Abstreiter and A. Fontcuberta i Morral, *Phys. Rev. B*, 2008, **77**, 155326.
24. J. Y. Tsao, *Materials Fundamentals of Molecular Beam Epitaxy*, Academic Press Inc., San Diego, CA., 1993.
25. G. B. Stringfellow, *Organometallic Vapor-Phase Epitaxy: Theory and Practice*, Academic Press Inc., San Diego, CA, 1999.
26. M. Kibria, S. Zhao, F. Chowdhury, Q. Wang, H. Nguyen, M. Trudeau, H. Guo and Z. Mi, *Nature communications*, 2014, **5**, 3825.
27. R. Lorenzo, J. Gwénoilé, B. Andres De Luna, T. Maria, W. Elias, H. J. François, S. Rudeesun, G. Elisabeth, L. Ludovic and H. Jean-Christophe, *Nanotechnology*, 2010, **21**, 425206.
28. T. Richter, H. L. t. R. Meijers, R. Calarco and M. Marso, *Nano Lett.*, 2008, **8**, 3056-3059.
29. R. S. Dowdy, C. Zhang, P. K. Mohseni, S. A. Fortuna, J.-G. Wen, J. J. Coleman and X. Li, *Opt. Mater. Express*, 2013, **3**, 1687-1697.
30. A. C. Chia, J. P. Boulanger and R. R. LaPierre, *Nanotechnology*, 2013, **24**, 045701.
31. G. Imamura, T. Kawashima, M. Fujii, C. Nishimura, T. Saitoh and S. Hayashi, *Nano Lett.*, 2008, **8**, 2620-2624.
32. B. Ketterer, E. Uccelli and A. Fontcuberta i Morral, *Nanoscale*, 2012, **4**, 1789-1793.
33. S. Zhang, F. J. Lopez, J. K. Hyun and L. J. Lauhon, *Nano Lett.*, 2010, **10**, 4483-4487.
34. K. Jeganathan, R. K. Debnath, R. Meijers, T. Stoica, R. Calarco, D. Grutzmacher and H. Luth, *J. Appl. Phys.*, 2009, **105**, 123707-123705.
35. T. Stoica and R. Calarco, *IEEE J. Sel. Topics Quantum Electron.*, 2011, **17**, 859-868.
36. R. Mata, A. Cros, K. Hestroffer and B. Daudin, *Phys. Rev. B*, 2012, **85**, 035322.
37. J. Wang, F. Demangeot, R. Péchou, A. Ponchet, A. Cros and B. Daudin, *Phys. Rev. B*, 2012, **85**, 155432.
38. I. Kunie, K. Keiko, O. Naoki, H. Hajime, K. Masahiro and P. Hrvoje, *Journal of Physics: Condensed Matter*, 2013, **25**, 205404.
39. F. Furtmayr, M. Vilemeyer, M. Stutzmann, J. Arbiol, S. Estrade, F. Peiro, J. R. Morante and M. Eickhoff, *J. Appl. Phys.*, 2008, **104**, 034309-034307.
40. A. Jordi, E. Sónia, D. P. Joan, C. Albert, F. Florian, S. Christoph, L. Andreas, S. Martin, E. Martin, H. G. Mhairi, L. B. Andrew, P. Francesca and R. M. Joan, *Nanotechnology*, 2009, **20**, 145704.
41. H. Hiroshi, *Journal of Physics: Condensed Matter*, 2002, **14**, R967.
42. A. Kaschner, H. Siegle, G. Kaczmarczyk, M. Strassburg, A. Hoffmann, C. Thomsen, U. Birkle, S. Einfeldt and D. Hommel, *Appl. Phys. Lett.*, 1999, **74**, 3281-3283.

-
43. G. Kaczmarczyk, A. Kaschner, A. Hoffmann and C. Thomsen, *Phys. Rev. B*, 2000, **61**, 5353-5357.
44. H. Harima, T. Inoue, S. Nakashima, M. Ishida and M. Taneya, *Appl. Phys. Lett.*, 1999, **75**, 1383-1385.
- 5 45. H. Harima, T. Inoue, Y. Sone, S. Nakashima, M. Ishida and M. Taneya, *Phys. Status Solidi B*, 1999, **216**, 789-792.
46. S. Tripathy, S. J. Chua, A. Ramam, E. K. Sia, J. S. Pan, R. Lim, G. Yu and Z. X. Shen, *J. Appl. Phys.*, 2002, **91**, 3398-3407.
47. A. Hoffmann, A. Kaschner and C. Thomsen, *Phys. Status Solidi C*,
10 2003, **0**, 1783-1794.
48. R. Kirste, M. P. Hoffmann, J. Tweedie, Z. Bryan, G. Callsen, T. Kure, C. Nenstiel, M. R. Wagner, R. Collazo, A. Hoffmann and Z. Sitar, *J. Appl. Phys.*, 2013, **113**, 103504-103505.
49. C. I. Wu, A. Kahn, N. Taskar, D. Dorman and D. Gallagher, *J. Appl.*
15 *Phys.*, 1998, **83**, 4249-4252.
50. J. P. Long and V. M. Bermudez, *Phys. Rev. B*, 2002, **66**, 121308.
51. H. Sezen, E. Ozbay, O. Aktas and S. Suzer, *Appl. Phys. Lett.*, 2011,
98, 111901.
52. M. Foussekis, J. D. McNamara, A. A. Baski and M. A. Reshchikov,
20 *Appl. Phys. Lett.*, 2012, **101**, 082104.
53. K. M. Tracy, W. J. Mecouch, R. F. Davis and R. J. Nemanich, *J. Appl. Phys.*, 2003, **94**, 3163-3172.